Validation of Classical Transport Cross Section for Ion-Ion Interactions Under Repulsive Yukawa Potential

Tian-Xing Hu,[1] Dong Wu,[1, a)] C. L. Lin,[2, 1] Z. M. Sheng,[3] B. He,[2, b)] and J. Zhang[1, 4]

[1)]*Key Laboratory for Laser Plasmas and School of Physics and Astronomy, and Collaborative Innovation Center of IFSA, Shanghai Jiao Tong University, Shanghai, 200240, China*

[2)]*National Key Laboratory of Computational Physics, Institute of Applied Physics and Computational Mathematics, Beijing 100088, People's Republic of China.*

[3)]*Institute for Fusion Theory and Simulation, Department of Physics, Zhejiang University, Hangzhou 310027, China.*

[4)]*Institute of Physics, Chinese Academy of Sciences, Beijing 100190, China.*

Value of cross section is a fundamental parameter to depict the transport of charged particles in matters. Due to masses of orders of magnitude higher than electrons and convenience of realistic calculation, the cross section of elastic nuclei-nuclei collision is usually treated via classical mechanics. The famous Bohr criterion was firstly proposed to judge whether the treatment via classical mechanics is reliable or not. Later, Lindhard generalized the results of Coulomb to screening potentials. Considering the increasing importance of detailed ion-ion interactions under modern simulation codes in inertial confinement fusion (ICF) researches, the validation of classical transport cross section for ion-ion interactions in a big range of parameter space is certainly required. In this work, the transport cross sections via classical mechanics under repulsive Yukawa potential are compared with those via quantum mechanics. Differences of differential cross sections are found with respect to scattering angles and velocities. Our results generally indicate that the classical picture fails at the cases of both low and high velocities, which represent a significant extension of the famous Bohr criterion and its generalized variations. Furthermore, the precise validation zones of classical picture is also analysed in this work. This work is of significant importance for benchmarking the modern ion-kinetic simulation codes in ICF researches, concerning the stopping power of α particles in DT fuels, ion-ion friction and viscous effects in the formation of kinetic shocks.

I. INTRODUCTION

Ion-ion collision is of fundamental importance in inertial confinement fusion (ICF) researches[1–4]. For example, at the latter stage of ignition and burning ware propagation, more than a half of the energy of fusion α particles is deposit directly into DT ions through ion-ion collision[5]. Especially, at the end of range, the dominant stopping power of α particles comes from ion-ion interactions, in which both deflections and decelerations need to be taken seriously. In terms of modern ion-kinetic simulation code, accurate modelling of ion-ion collisions is vital, for example, the Monte-Carlo collision method widely used in PIC or hybrid-PIC code[6–8] require an explicit and "easy-to-handle" ion-ion transport cross section.

In most of the literatures, the ion-ion collision is treated via classical approaches. Due to the increasing importance of detailed ion-ion interactions under modern ion-kinetic simulation codes in ICF researches, the validation of classical transport cross section for ion-ion interactions in a big range of parameter space is certainly required.

Transport cross-section (TCS) is the basis in order to model ion-ion collisions[9]. For matters at room temperature or plasmas, the TCS is usually calculated based on integration of two classical particles[10], where quantum mechanical effects are often neglected.

In the pioneering work of N. Bohr[11], a criterion on the applicability of classical orbital picture in the calculation of Coulomb scattering was proposed, and it is called the Bohr criterion nowadays. The Bohr criterion was then generalized by Lindhard to the case of the screened field such as the standard atomic potential[12] in 1965, and to the case of Yukawa potential later[9]. Both Bohr and Lindhard's works were based on small angles approximations and suggested that the classical orbital picture fail at high velocities. However the contribution of all the scattering angles must be included to get the TCS.

TCS is usually defined as

$$\sigma_{\text{tr}}(v) = \int (1 - \cos\theta)\sigma(\theta, v)\mathrm{d}\Omega, \tag{1}$$

where $\sigma(\theta, v)$ is the differential cross-section (DCS) with θ the scattering angle at the frame of centre of mass when the relative velocity between the projectile and the target particle is v. In most of the literatures and articles[6,13,14], when it comes to ion-ion collision, the classical method is often just taken for granted without any justification. To our knowledge, only E. Bonderup[10] offered a brief analysis of this issue based on the Linhard standard potential for small-angle scattering. Bouderup qualitatively concluded that the classical orbital picture fails at large collision parameter or small scattering angle, at which the contribution to stoppig power is negligible, but did not give a quantitative comparison. Moreover, he also pointed out that this is true for any other potentials.

The repulsive Yukawa potential is widely used to describe the

---

a)Electronic mail: dwu.phys@sjtu.edu.cn
b)Electronic mail: he_bin@iapcm.ac.cn

ion-ion interaction in plasma physics researches. The calculation of classical TCS under Yukawa potential is much simpler than that of quantum TCS, the reliability of which is very important to the research of the transportion of charged particles. Despite being a fundamental problem, the quantitatively comparison between the quantum and classical result is currently lacking.The main purpose of this paper is to discuss the applicability or the scope of application of Bohr's criterion to the TCS due to ion ion collison under Yukawa potential in detail. It is found that the classical collision picture is failed at both very low and high velocity cases. In the work we will take the example of the collisons of different charge state ions with DT ion to study the validity of classical TCS. Some numerical results are presented for a few screening lengths of the Yukawa potential since no analytical expressions can be found for the potential.

The paper is organized as following. In Sec. II, we briefly introduce the classical and quantum mechanical methods in the calculation of TCS involved in this paper. In Sec. III and IV, we use these numerical methods to test the validity of the generalized Bohr's criterion for DCS and TCS, respectively. And finally the conclusions are presented in the last section. The atomic units are used throughout the work unless otherwise explicitly indicated.

II.   METHOD

Firstly, we briefly review the classical and quantum mechanical methods for calculating the DCS and TCS. In the work the potential for binary collision is always the Yukawa potential $U(r) = \frac{Z_1 Z_2}{r} e^{-r/\lambda_0}$. Here λ_0 is the characteristic screening length. And Z_1 and Z_2 ($Z_1 Z_2 > 0$) are the charges for the projectile and the target ion, respectively.

A.   Classical Scattering

The classical scattering angle under the potential $U(r)$ is given by

$$\theta(b) = \pi - 2b \int_{r_0}^{\infty} \frac{\mathrm{d}r/r^2}{\sqrt{1 - b^2/r^2 - U(r)/\mathscr{E}}}, \quad (2)$$

where b is the collisional parameter, r_0 is the apsis of the scattering, and $\mathscr{E} = \mu v^2/2$, with μ being the effective mass $m_1 m_2/(m_1 + m_2)$, is the incident energy. Here m_1 and m_2 are the masses for the projectile and the target ion, respectively. With the change of variable[15]

$$u = \sqrt{\frac{r_0}{r} - 1}, \quad (3)$$

Eq. (2) become

$$\theta(b) = \pi - 4b \int_0^1 \frac{\mathrm{d}u}{\sqrt{g(u)}}, \quad (4)$$

where

$$g(u) = b^2 \left(2 - u^2\right) + \frac{r_0^2}{u^2 \mathscr{E}} \left[U(r_0) - U \left(\frac{r_0}{1 - u^2} \right) \right]. \quad (5)$$

Thus, the singularity at the apsis r_0 is avoided. The differential cross-section (DCS) is then

$$\sigma(\theta) = \frac{b}{\sin\theta} \left| \frac{\mathrm{d}b}{\mathrm{d}\theta} \right|. \quad (6)$$

B.   Quantum Scattering

We will introduce three major quantum mechanical methods involved in this paper. Firstly, the Born approximation is the perturbation method for quantum scattering processes. We consider only the first-order approximation in this paper, and the result serves as a benchmark of our numerical results in high-velocity limit. Secondly, the partial wave method (PWM) is the standard approach which calculates the DCS/TCS by expanding the scattering wave into a series of spherical harmonics and then solve the phase shifts order by order. Since the scattering amplitude would eventually tends to zero provided the quantum number ℓ is large enough, we can obtain a result with any satisfactorily accuracy by means of the PWM. Lastly, the WKB approximation is an semi-classical method of the wave equation i.e., the approximation of geometric optics, which is easier to calculate at both middle and high velocity regime than the exact PWM.

1.   Born Approximation

For the Yukawa potential the scattering cross-section calculated via Born approximation $\sigma_{\mathrm{Born}}^{\mathrm{Y}}(\theta)$, which is only valid in high velocity limit, is related to the Rutherford expression

$$\sigma^{\mathrm{C}}(\theta) = \frac{b_0^2}{4\sin^4 \frac{\theta}{2}} \quad (7)$$

by

$$\sigma_{\mathrm{Born}}^{\mathrm{Y}}(\theta) = \sigma^{\mathrm{C}}(\theta) \left(1 + \frac{1}{q^2 \lambda_0^2} \right)^{-2}, \quad (8)$$

where

$$q = 2k\sin\frac{\theta}{2} \text{ and } b_0 = \frac{Z_1 Z_2}{\mu v^2}, \quad (9)$$

are the momentum transfer for each collision and the collision radius (which represents the $90°$ deflection impact parameter for classical coulomb collision) respectively. And $k = \mu v$ stands for the momentum of the collision system. From these the total cross section is

$$\sigma_{\mathrm{tot}} = \frac{16\pi\mu^2 \lambda_0^2 Z_1^2 Z_2^2}{1 + 4\mu^2 v^2 \lambda_0^2}, \quad (10)$$

When v is high enough, it becomes $4\pi\lambda_0^2 Z_1^2 Z_2^2/v^2$.

2. Partial Wave Method

The exact solution of the phase shift obeys the differential equation[16]

$$\frac{\mathrm{d}\delta_\ell}{\mathrm{d}r} = -\frac{2\mu U}{k}\left[\hat{j}_\ell(kr)\cos\delta_\ell - \hat{n}_\ell(kr)\sin\delta_\ell\right]^2, \qquad (11)$$

and the scattering amplitude is

$$f(\theta) = \sum_{\ell=0}^{\infty} f_\ell(\theta) = \frac{1}{k}\sum_{\ell=0}^{\infty}(2\ell+1)e^{i\delta_\ell}\sin\delta_\ell P_\ell(\cos\theta). \quad (12)$$

and

$$\sigma(\theta) = |f(\theta)|^2. \qquad (13)$$

One can calculate the transport cross-section directly by the phase shift[17]:

$$\sigma_{\mathrm{tr}}(v) = \frac{4\pi}{k^2}\sum_{\ell=0}^{\infty}(\ell+1)\sin^2\left(\delta_\ell - \delta_{\ell+1}\right), \qquad (14)$$

instead of by Eq. (1). Certainly it is impossible to consider the infinite number of partial waves, however, in practice, only a few of them contribute to very low velocity collisions.

3. Approximation Method

As the relative velocity v increases, more and more partial waves should be taken into consideration, and it is difficult to solve equation (11) for high ℓ waves. In such cases, the WKB approximation is therefore a very good approximation[18]:

$$\delta_\ell^{\mathrm{WKB}} = \int_{r_1}^{\infty}\mathrm{d}r\sqrt{k^2 - \frac{(\ell+1/2)^2}{r^2} - 2\mu U(r)} \\ - \int_{r_0}^{\infty}\mathrm{d}r\sqrt{k^2 - \frac{(\ell+1/2)^2}{r^2}}, \qquad (15)$$

where r_0 and r_1 are the apsis of free and scattering particles respectively.

On the other hand, for very large ℓ, the Legendre function $P_\ell(\cos\theta)$ in Eq. (12) are highly-oscillatory, which makes it difficult the calculate scattering amplitude $f(\theta)$. Our solution is to cut-off the summation at ℓ_b, and let

$$f(\theta) = \sum_{\ell=0}^{\ell_b} f_\ell^{\mathrm{WKB}}(\theta) - \sum_{\ell=0}^{\ell_b} f_\ell^{\mathrm{Born}}(\theta) + f^{\mathrm{Born}}(\theta), \qquad (16)$$

which means we use the Born approxiamtion results of f_ℓ's for $\ell > \ell_b$ components[2]. Here,

$$f^{\mathrm{Born}}(\theta) = -\frac{2\mu}{q}\int_0^{\infty} rU(r)\sin qr\,\mathrm{d}r, \qquad (17)$$

and[19]

$$f_\ell^{\mathrm{Born}}(\theta) = -\frac{\pi(2\ell+1)}{2k}P_\ell(\cos\theta)\int_0^{\infty} rU(r)J_{\ell+\frac{1}{2}}^2(kr)\mathrm{d}r. \quad (18)$$

The integration containing a Bessel function in Eq. (18) has an analytical form:

$$\int_0^{\infty} rU(r)J_{\ell+1/2}^2(kr)\mathrm{d}r = \frac{(2k)^{2\ell+1}\lambda_0^{2\ell+2}}{\pi} \\ \times B(\ell+1,\ell+1)\,_2F_1(\ell+1,\ell+1;2\ell+2;-4k^2\lambda_0^2), \qquad (19)$$

where $_aF_b$ is the generalized hypergeometic function of order a, b. Eq. (16) becomes exact when ℓ_b is large enough such that $\delta_{\ell_b}^{\mathrm{WKB}} \simeq \delta_{\ell_b}^{\mathrm{Born}}$.

III. DIFFERENTIAL CROSS-SECTION DUE TO ION-ION COLLISION

In this section, we generalize the original Bohr's criterion, which is derived based on small angle Coulomb scattering, to a more general criterion that applies to arbitrary potentials and deflection angles. This criterion is then benchmarked for DCS under repulsive Yukawa potential by numerical methods.

A. The Generalized Bohr Criterion

In 1948, N. Bohr proposed a famous criterion for the validity of the classical orbital picture, now known as the Bohr criterion[11], which is[12]

$$\frac{1}{\mu v}\left|\frac{\mathrm{d}}{\mathrm{d}b}\theta^{-1}\right| \ll 1, \qquad (20)$$

where b is the collision parameter. For a small angle Coulomb scattering ($\theta \ll 1$), it becomes

$$\frac{2Z_1Z_2}{v} = \frac{2b_0}{\lambda} \equiv \kappa \gg 1, \qquad (21)$$

which means that the collision radius b_0 should be much larger than the de Broglie wave length $\lambda = 1/\mu v$. The Bohr's formula Eq. (21) implies that the quantum effect appears at high velocity ($v > 2|Z_1Z_2|$) case for Coulomb scattering, as is pointed out by Bounderup[10], this is because the equation requires that $b_0 \gg \lambda$, and b_0 is proportional to v^{-2} whereas λ is proportional to v^{-1}.

The original Bohr's criteron (21) is independent of the collisional parameter b. Following Bohr's idea, generally, the following expression from Eq. (20)

$$\kappa \gg 2\left|b_0\frac{\mathrm{d}}{\mathrm{d}b}\frac{1}{\theta}\right| \qquad (22)$$

can be regarded as the criterion for arbitrary binary collisions with any form of interactions, which should be dependent on

the collisonal parameter. For example, for small angle scatterings with repulsive Yukawa potentials ($\sim \mathrm{e}^{-r/\lambda_0}/r$), the deflection angle can be approximated by[9]

$$\theta(b) = \frac{2b_0}{\lambda_0} K_1\left(\frac{b}{\lambda_0}\right), \qquad (23)$$

with which Eq.(22) (called as the general Bohr criterion (GBC) in the following) reduces to[9]

$$\kappa \gg \lambda_0 \frac{\mathrm{d}}{\mathrm{d}b} K_1^{-1}\left(\frac{b}{\lambda_0}\right). \qquad (24)$$

where $K_\nu(x)$ is the ν's order modified Bessel function of the second kind. For collisions with not very low velocity, another approximation was proposed in Ref. [17]:

$$\theta(b) = 2\arctan\left[\frac{b_0}{\lambda_0} K_1\left(\frac{b}{\lambda_0}\right)\right], \qquad (25)$$

which works well when $v \gtrsim 10^{-4}$ for ion-ion collision as found by us. When $b \ll \lambda_0$, $\frac{b_0}{\lambda_0}K_1\left(\frac{b}{\lambda_0}\right)$ becomes $\frac{b_0}{b}$. In this case $\theta(b) = 2\arctan\left[\frac{b_0}{b}\right]$, which is just the result of strict Coulomb scattering.

B. Numerical Benchmark for DCS

1. Results of the Generalized Bohr's Criterion

Here, by means of the numerical method mentioned in the last section, we calculated the right-hand-side of Eq. (22) as a function of collision parameter b for the scattering process in DT plasmas. The target particle is assumed to be an effective particle with $Z_2 = 1$ and $m_2 = 2.5m_p$, where m_p is the mass of a proton. For simplicity, $m_1 = 2Z_1m_p$ is chosen. In Fig. 1 (a) the y-axis is b/λ_0, and the three lines are the classical valid boundary $b = b_c(v)$ obtained by solving the equation

$$\kappa = 2b_0 \left|\frac{\mathrm{d}}{\mathrm{d}b} \frac{1}{\theta(b_c)}\right|, \qquad (26)$$

at three different screening lengths and beyond which the classical orbital picture is no longer valid. Fig. 1 (b) plotted the deflection angle boundary $\theta = \theta_c(v)$ calculated with the corresponding collision parameter in Fig. 1 (a). It should be mentioned that Eq. (26) is not the real form of GBC since later we will find that GBC is too strong to determine the range of b or θ where the classical meachnics can be applied under the Yukawa potential. Four behaviours can be seen from Fig. 1:

1. When $v < 2|Z_1Z_2|$, θ_c (b_c) decreases(increases) as λ_0 increases, and becomes 0 (∞) for Coulomb potential when $\lambda_0 \to \infty$.

2. There are two velocity boundaries depending on the impact parameter, below which the classical picture is valid. The fisrt ($v = 2|Z_1Z_2|$) is refered to as the
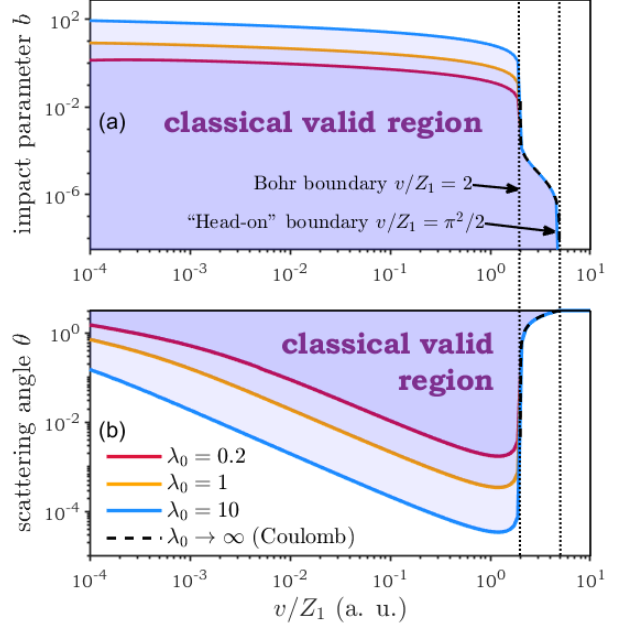

Figure 1. (a) The critical value of collision parameter (b_c) at different v, beyond which the classical orbital picture is no longer valid according to the Bohr criterion Eq. (22). (b) The deflection angle θ corresponding to the critical collision parameter b_c at different v. In both panels, $Z_1 = 2$ is fixed, and λ_0 is equal to 0.2, 1.0, and 10.0, respectively.

"Bohr boundary", while the second ($v = \pi^2|Z_1Z_2|/2$) the "head-on boundary", since θ_c at this boundary is equal to π. When $v > \pi^2|Z_1Z_2|/2$ no solution of b for Eq. (26) can be found, which means that the classical picture is invalid for this region.

3. When v changes from 10^{-4} to $2|Z_1Z_2|$, $b_c(v)/\lambda_0$ is almost independent of λ_0, while θ_c decreases as λ_0 increases.

4. When $v > 2|Z_1Z_2|$, both θ_c and b_c are independent upon λ_0, and the b_c's for both Coulomb potential and Yukawa potentials are almost coincide.

We will explain these behaviors one by one as follows:

1. When the impact parameter is large, the strength of Yukawa potential decreases rapidly, while the strength of Coulomb potential decreases slowly. Specifically, when $b \gg \lambda_0$, Eq. (25) reduce to

$$\theta(b) = 2\arctan\left[\frac{b_0}{\lambda_0}\sqrt{\frac{\pi\lambda_0}{2b}}\exp\left(-\frac{b}{\lambda_0}\right)\right], \qquad (27)$$

which is very different from the Coulomb scattering. This means that both b_c and $theta_c$ are dependent upon λ_0 in the case.

2. The "Bohr boundary" $v = 2|Z_1 Z_2|$ is exactly what Bohr's original criterion predicted, which is obtained under small angle approximation. As the scattering angle increases, the boundary becomes larger, and reach to the "head-on" boundary when $\theta_c = \pi$. We calculate the head-on boundary here. Solving the boundary equation

$$\frac{1}{\mu v}\left|\frac{\mathrm{d}}{\mathrm{d}b}\theta^{-1}\right| = 1 \tag{28}$$

in oreder to obtain b_c for Yukawa potential, we get

$$\frac{b_0\left[K_0\left(\frac{b_c}{\lambda_0}\right) + K_2\left(\frac{b_c}{\lambda_0}\right)\right]}{4k\lambda_0^2\left(1 + \frac{b_1^2}{\lambda_0^2}\right)\arctan\left(\frac{b_1}{\lambda_0}\right)^2} = 1, \tag{29}$$

where

$$b_1 \equiv \frac{Z_1 Z_2}{\mu v^2}K_1\left(\frac{b_c}{\lambda_0}\right). \tag{30}$$

For head-on collision b should be very small so that $b_c \ll \lambda_0$ and $b_1 \simeq \lambda_0 b_0/b_c$, and by applying $K_0(x) \simeq -\ln x$, $K_1(x) \simeq x^{-1}$, and $K_2(x) \simeq 2x^{-2}$, we obtain

$$\frac{b_0}{2k\left(b_0^2 + b_c^2\right)\arctan\left(b_0/b_c\right)^2} = 1. \tag{31}$$

Numerical calculation also shows that $b_0^2 \gg b_c^2$ is generally true when $v > 2|Z_1 Z_2|$, hence Eq. (31) reduces to

$$\frac{v}{|Z_1 Z_2|} = 2\arctan\left(\frac{b_0}{b_c}\right)^2. \tag{32}$$

Since $\arctan\left(b_0/b_c\right)^2 \leq \pi^2/4$, v should not be more than $|Z_1 Z_2|\pi^2/2$, which explains the head-on boundary.

3. Fig. 1 (a) tells us that when $v < 2|Z_1 Z_2|$, $b_c \gg \lambda_0$ or $b_c \simeq \lambda_0$, which means b_1 may be greater or smaller than λ_0. If $b_1 < \lambda_0$, we have $\arctan\left(b_1/b_c\right) \simeq b_1/b_c$ and $1 + b_1^2/\lambda_0^2 \simeq 1$, then Eq. (29) reduces to

$$\frac{b_0}{4kb_1^2}\left[K_0\left(\frac{b_c}{\lambda_0}\right) + K_2\left(\frac{b_c}{\lambda_0}\right)\right] = 1. \tag{33}$$

Similarily, if $b_1 > \lambda_0$, then $\arctan(b_1/\lambda_0)$ is ranging from $\pi/4$ to $\pi/2$, and becomes weakly dependent on b_1/λ_0. Thus we approximately let $\arctan(b_1/\lambda_0)$ equal to a constant C. Eq. (29) thus becomes

$$\frac{b_0}{4kb_1^2 C^2}\left[K_0\left(\frac{b_c}{\lambda_0}\right) + K_2\left(\frac{b_c}{\lambda_0}\right)\right] = 1. \tag{34}$$

Obviously in these two cases the solution is dependent on b_c/λ_0, not λ_0 if we notice that $\frac{b_0}{4kb_1^2} = \frac{v}{4|Z_1 Z_2|K_0^2\left(\frac{b_c}{\lambda_0}\right)}$ in the above two equations. This explains the observed second behavior. Also thus indicates that b_c is independent on reduced mass μ.
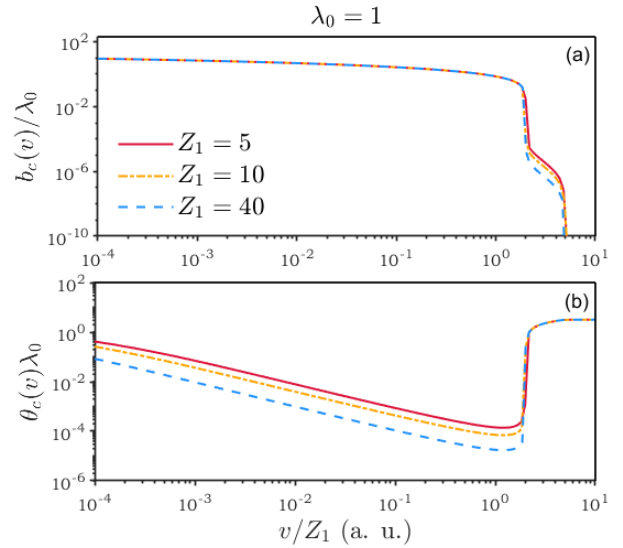

Figure 2. (a) The critical value of collision parameter (b_c) at different v/Z_1. (b) The deflection angle θ corresponding to the critical collision parameter b_c at different v/Z_1. in both panels λ_0 is fixed to be 1.0, and three different projectile charge states with Z_1 equal to 5, 10 and 40 are chosen.

4. The boundary value b_c and θ_c for $v > 2|Z_1 Z_2|$ is determined by Eq. (31), which is independent of λ_0. This is also the boundary of v for large angle Coulomb scattering since $\theta(b)$ for Debye potential becomes that for Coulomb potential in the case.

Now it is necessary for us to further discuss the behavior of θ_c in Fig. 1 (b.) From the figure we found that, θ_c depends on λ_0 and decreases with v when $v < 2|Z_1 Z_2|$, and θ_c rapidly rises up to π for higher v. This is easy to see if Eq. (25) is noticed. The equation means that the scattering angle is a function of λ_0 when $b \ll \lambda_0$ is not satisfied (since $K_1(x) \simeq x^{-1}$ for small x), which correspounds to the case for $v < 2|Z_1 Z_2|$ from Fig. 1 (a). For $v > 2|Z_1 Z_2|$ due to that b_c is very small or even smaller than b_0, the corresponding scattering angle becomes large and even close to π. Besides this, θ_c is decreasing with λ_0 rising when $v < 2|Z_1 Z_2|$, which is understandble from the equation since b_c/λ_0 is almost independent on λ_0 and decreases with v in the case. In addition, b_0 rapidly decreases with v increasing, which results in the reducing of θ_c at the same time according to the equation when $v < 2|Z_1 Z_2|$.

The above analyses are further embodied in Fig. 2 (a) and Fig. 2 (b), where the evolutions of b_c/λ_0 and θ_c with v/Z_1 are shown, respectively when $Z_1 = 5$, 10, and 40 for λ_0 fixed to be 1.0. Here the explanation of the figure will be given no longer. Similar results with the figure for many other Z_1 and λ_0 have also been obtained and not shown here.

2. Comparison of Classical and Quantum DCS

So far we have presented the range of b or θ where the classical meachnics can be applied under the Yukawa potential
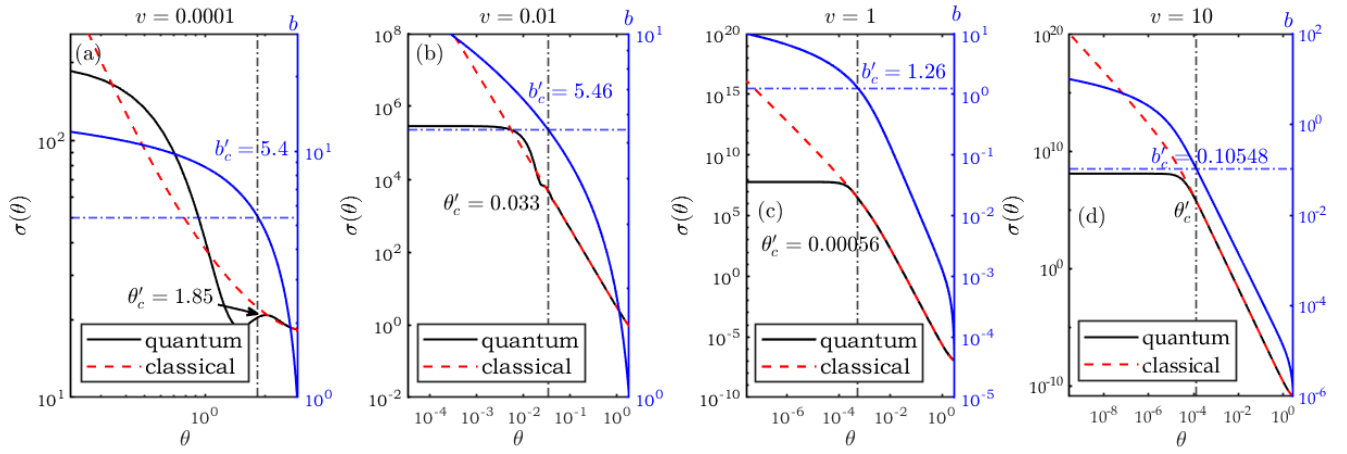
Figure 3. Variations of impact paramter b, classical and quantum differential cross sections with scattering angle θ when $v = 10^{-4}$, 10^{-2}, 1.0, and 10.0. Here $Z_1 = 2.0$ and $\lambda_0 = 1.0$ are chosen. Both b'_c and corresponding angle θ'_c are marked, where b'_c is where the classical and quantum differential cross-section starting to disagree (about 2% deviation).

according to Eq. (26) related to Bohr criterion. The reliability of the result need be tested by the comparison of classical and quantum DCS. For this aim we now first take a look at the DCS by both classical and qunatum methods. In order to calculate the DCS by means of Eq. (13), we take the result of PW method as the exact quantum mechanical phase shift if there is a substantial difference between the PW and the WKB results. Fig. 3 shows both the results of classical and quantum DCS as a function of scattering angle θ when $v = 10^{-4}$, 10^{-2}, 1.0, and 10.0. Here $Z_1 = 2.0$ and $\lambda_0 = 1.0$ are chosen. The relevant variations of impact paramter b with θ are also plotted. Obviously the DCS calculated via the two methods are almost identical for relatively large deflection angle θ, and their difference appears obviously with the decreasing of θ or corresponding to bigger impact parameter. Morever, the quantum result converges to a finite value as $\theta \to 0$ while the classical result does not, which means that the classical total cross section is divergent while the quantum result is not. We then select a specific deflection angle θ'_c, at which the quantum and classical results just begin to deviate about 2%, and set the corresponding collision parameter as the actual critical collision parameter b'_c which may be different from b_c. For the case of $Z_1 = 2$, $\lambda_0 = 0.2$, 1.0, and 10.0 all the b'_c and b_c are plotted in Fig. 4. Three features can be seen from the figures:

1. When v is smaller than 10^{-3}, b'_c and b_c does not match very well.

2. When v is between 10^{-3} to 1, b'_c and b_c are close to each other.

3. When v is approaching or beyond $2|Z_1 Z_2|$, b'_c and b_c become to match no longer.

And so does θ_c and θ'_c. Again, we explain them one by one here:

1. When v is very small ($< 10^{-3}$), the quantum and classical DCS is different in the most range of θ, it is difficult to obtain a critical deflection angle θ'_c and thus
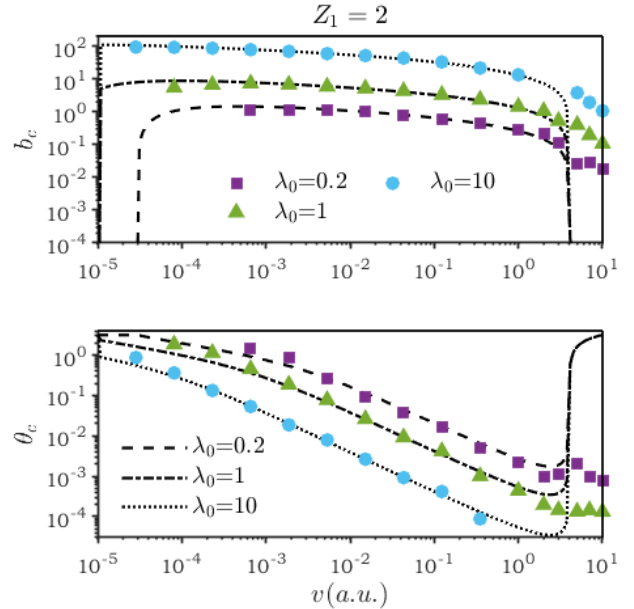

Figure 4. Variations of b'_c / θ'_c (markered lines) and b_c / θ_c (unmarkered lines) as a function of v for $\lambda_0 = 0.2$, 1, and 10 when $Z_1 = 2.0$

the critical collision parameter b'_c. In this case we think the quantum wave character plays its dominant role to determine the DCS and the concept of classical impact parameter, which was used in Bohr criterion, is invalid. The reason is that the corresponding de Broglie wave length $\lambdabar > 3.54$ for the collision system, which is smaller than the screening lengths λ_0 in the figure. This makes $k\lambda_0 = \frac{\lambda_0}{\lambdabar} < 1$. In other words, only very few number of partial wave l has contribution to the quantum DCS.

2. The second feature confirms that the physical interpretation of θ_c is indeed the critical value of scattering an-

gle below which the quantum and classical DCS starting to deviate. Meanwhile the GBC will results in a range of much smaller b or much bigger θ that the classical mechanics can be applied. In other words, in the case the GBC is too strong to get a proper range wher the clasical picture is reliable.

3. We think that in the case both the GBC and its weaker form Eq. (26) are invalid to give a proper value of θ below which the classical mechanics does not work though we are not clear to this. In fact only in the range of very small θ or enough big b the classical and quantum DCSs become different. This has something to do with the failure of Bohr criterion for the scattering under Coulomb potential. It is well known that the two DCSs by both classical and quantum mechanics are always the same for Coulomb potential[20] while the original Bohr criterion suggest that the classical picture fails when $v \ll 2|Z_1 Z_2|$. The difference between Coulomb and Yukawa potentials occurs when $r > \lambda_0$. In scattering it corresponds to enough large b or small θ, which is just the range where the classical picture does not work.

Furthermore, for the case of high enough velocity the discrepancy between the two DCSs by both classical and quantum mechanics can be seen from the related analytic expressions. The corresponding classical Yukawa DCS is[17]

$$\sigma(\theta) = \sigma^C(\theta) \frac{x K_1^3(x)}{|dK_1/dx|}, \tag{35}$$

which reduces to the Coulomb cross-section $\sigma^C(\theta)$ when $x \equiv b/\lambda_0$ is small enough. However, for ion-ion collision in high speed $b_0 \ll \lambda_0$ so that the corresponding θ for such x covers a large range from small angle to π For quantum mechanical Born approxiamtion Eq. (8) also usually reduces to $\sigma^C(\theta)$ only if θ is not very small. All these mean that the discrepancy between the two DCSs by both classical and quantum mechanics only appears for very small *theta*, as shown in the above two figures. This further varifies that the GBC fails in the case.

IV. RESULTS OF THE TRANSPORT CROSS-SECTION

The transport cross-section is what really matters in a collision-based method[21]. In the section we first analyse the asymptotic behaviour of the integrands for classical and quantum TCS in low and high velocity limits, and then test the analysis by numerical results of both classical and quantum results of TCS.

A. Low Velocity Case

In the classical calculations, the transport cross-section depends not only on the differential cross section $\sigma(\theta, v)$, but also the factor $(1 - \cos\theta)\sin\theta$, according to Eq. (1). We calculate integrand of Eq. (1) with the same parameter used in the previous section, the result plotted in Fig. 5, where the critical deflection angle θ_c is the corresponding angle to the critical collision parameter presented in the last section. As we can see, at very low collision velocity ($v = 0.0001$), the integrand of classical and quantum TCS is quite different with θ_c much bigger than θ, and the Bohr's criterion does not work well at such low velocity as explained in the before.

B. Middle Velocity Case

For medium velocities ($v = 0.001, 0.01$, and even $v = 1.0$), the discrepancy of classical and quantum integrands of DCS become large only in small-θ region though they are suppressed by the $(1 - \cos\theta)\sin\theta$ factor. At higher θ the integrands thus approximately coincide with each other. Notice that the integrand in the range $0 \sim \theta_c$ only contribute 1.79%, 0.13%, and 0.08% to the final results of TCS for $v = 0.001$, $v = 0.01$ and $v = 1$ respectively, and this is the reason why the quantum and classical TCS results are almost coincide with each other even though the classical DCS is divergent while quantum DCS is not. Only in this case the Bounderup's view is valid.

By the way here for the above two cases we only show the results for $Z_1 = 2.0$ and $\lambda_0 = 1$. For other Z_1 and λ_0 similar results with the figure have also been found and not shown here.

C. High Velocity case

At high collision velocity, the Born approximation of the transport cross-section gives

$$\begin{aligned} \sigma_{\text{tr}}(v) =& 2\pi \int_0^{\pi} (1 - \cos\theta)\sin\theta \, \sigma_{\text{Born}}^{Y}(\theta) \, d\theta \\ =& 2\pi b_0^2 \left[\ln\left(1 + 4\mu^2 v^2 \lambda_0^2\right) - \frac{4\mu^2 v^2 \lambda_0^2}{1 + 4\mu^2 v^2 \lambda_0^2} \right] \\ \simeq& 4\pi b_0^2 \ln\left(\mu v \lambda_0\right), \end{aligned} \tag{36}$$

where in the last line we have assumed $\mu v \lambda \gg 1$. On the other hand, the classical calculation[17] predicts that when $\mu v \lambda / |Z_1 Z_2| \gg 1$,

$$\sigma_{\text{tr}}(v) \simeq 4\pi b_0^2 \ln\left(\frac{2\lambda_0}{b_0} e^{-\gamma - \frac{1}{2}}\right). \tag{37}$$

One find that Eq. (36) and Eq. (37) only coincident when $v/|Z_1 Z_2| \simeq e^{\gamma + \frac{1}{2}}/2$, which means that when

$$v > 1.468 |Z_1 Z_2|, \tag{38}$$

the classical and quantum TCS should be different.

To be specific, for high velocity collision, we can concentrate on the limit where $\theta \to 0$. At this limit, according to Eq. (8) the Born approximation DCS converge to a constant:

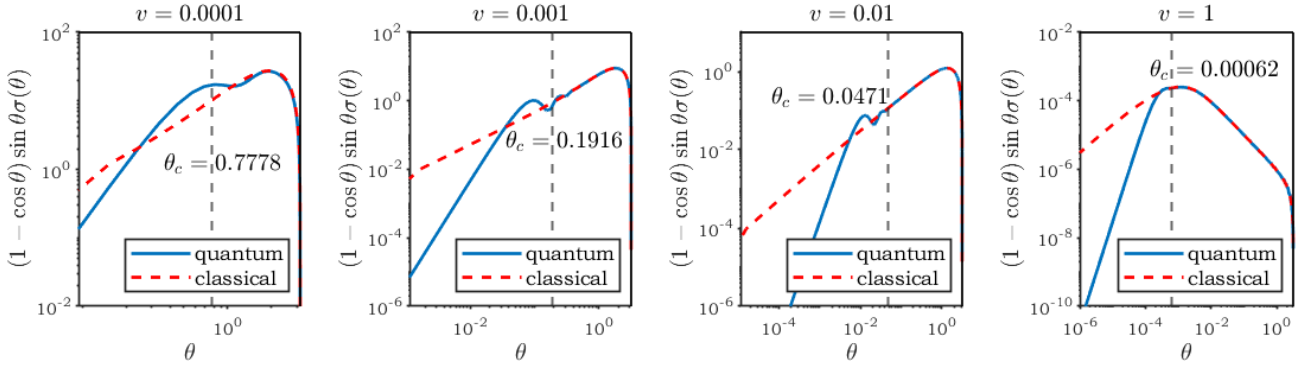$$\sigma(\theta \to 0) = 4 Z_1^2 Z_2^2 \mu^2 \lambda_0^2. \tag{39}$$

Figure 5. The integrands of TCS ($\lambda_0 = 1$) with $Z_1 = 2$ and $v = 10^{-4}, 10^{-3}, 10^{-2}$ and 1, where the solid-lines are quantum mechanical results and dashed-lines are classical with the corresponding θ_c marked.

Recall that the classical Yukawa DCS is[17]

$$\sigma(\theta) = \sigma^C(\theta) \frac{x K_1^3(x)}{|dK_1/dx|}, \tag{40}$$

where $x = b/\lambda_0$. Noticing that $K_n(x \gg 1) \simeq e^{-x}\sqrt{\pi/2x}$, we find that for $\theta \to 0$,

$$\sigma(\theta \to 0) = \frac{\pi}{2}\sigma^C(\theta)e^{-2x}$$
$$\simeq \frac{\pi}{2}\sigma^C(\theta)\exp\left[-LW\left(\frac{4\pi b_0^2}{\theta^2 \lambda_0^2}\right)\right], \tag{41}$$

where $LW(x)$ is the Lamberg W-function[22]. Therefore, the asymptotic behaviors of classical and quantum high-velocity DCS are quite different for very small angle scattering. However, in the following we will see that in the case the region of very small angle have an important contribution to the TCS although for other range of θ the quantum DCS is close to the classical one as mentioned in the endo of last section. In Fig. 6 the integrands in the total ranges of angles are plotted for two different high v with $v = 10$ and 100 at $Z_1 = 2$ and $\lambda_0 = 1$. It is easy to see that, despite that the Bohr criterion is absolutely violated at such high speed, there is still a large portion of the θ range where the classical and quantum DCS coincide. However, the contribution from the part of small angle to the TCS is important in this case. By integration it is found that contributions of the part with $\theta < 10^{-3}$ are about 26% of the total quantum TCS, and the discrepancy of DCS at $v = 10$ and 100 are 8.2% and 32% respectively.

D. Numerical Results of the TCS

In this subsection, the exact value of quantum and classical TCS are calculated by means of the aforementioned numerical methods. Notice that the classical TCS can be reduced to

$$\sigma_{\mathrm{tr}}(v) = 2\pi \int_0^\infty [1 - \cos\theta(v,b)]\, b\, db, \tag{42}$$

according to Eq. (6). The result is presented in Fig. 7, from which one can see that the quantum TCS and the classical TCS
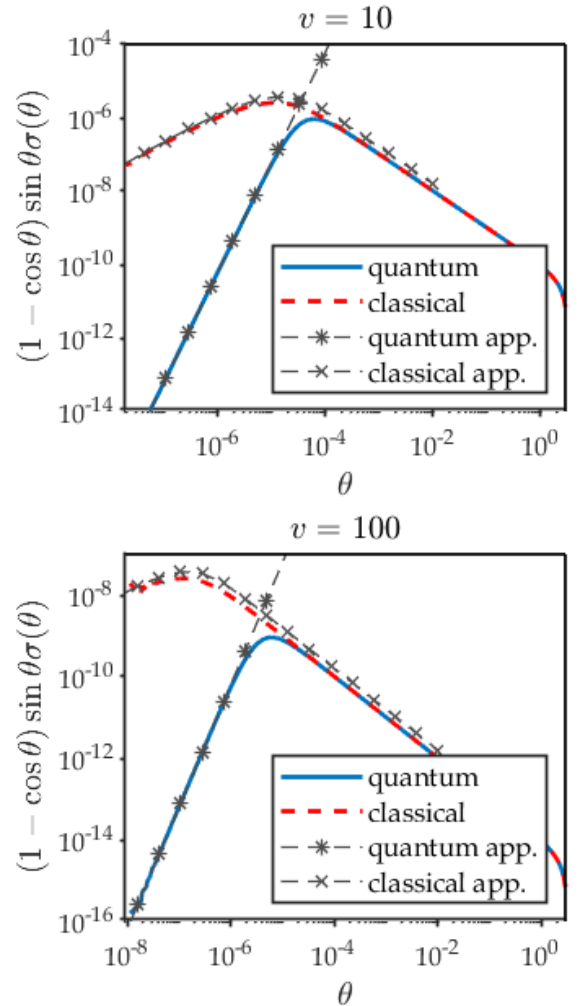

Figure 6. The integrands of TCS with $\lambda_0 = 1$ and $Z_1 = 2$ at high collision velocity ($v = 10, 100$), where the solid-lines are quantum mechanical results and dashed-lines are classical. The quantum and classical approximation curves are calculated via Eq. (39) and Eq. (41) respectively.
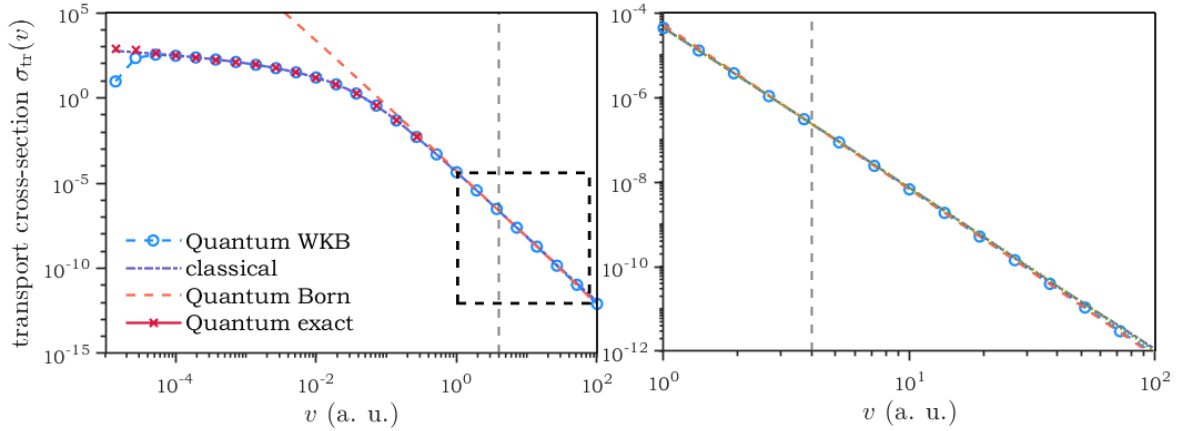
Figure 7. Transport cross-sections of ion-ion collision under Yukawa potential ($\lambda_0 = 1$ and $Z_1 = 2$) calculated via WKB approx., classical, Born approx., and exact partial wave method respectively. The dashed-line marks $v = 2|Z_1 Z_2| = 4$. The discrepancy in high-velocity range can be seen more clearly in the right panel.
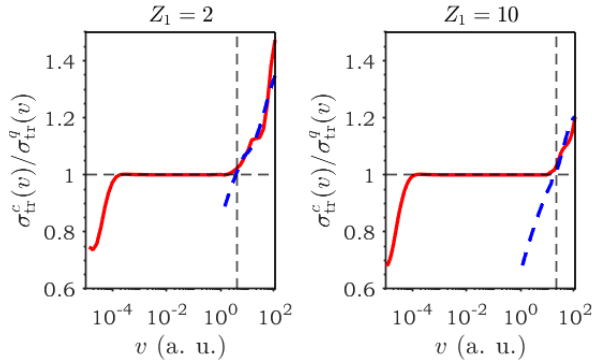

Figure 8. (Color online) The ratio of classical TCS to quantum one with $Z_1 = 2$ (a) and 10 (b) at $\lambda_0 = 1$. The red solid-line is calculated by numerical methods described in the context, and the blue dashed-line is the result from the approximation formulas Eq. (37) and Eq. (36).

coincide in the range of v between 10^{-3} and about $Z_1 Z_2$. In smaller v region, the WKB approximation result is obviously incorrect, let alone the Born approximation result. Hence, we choose the result of exact partial wave method to be the real quantum TCS in the case. In the larger v region, the classical and quantum (WKB) results deviate for each other a little bit, and the WKB result almost coincide with the Born approximation. This deviation takes places when $v > 2|Z_1 Z_2|$. In Fig. 8, we plotted the ratio of classical TCS to quantum TCS for two different projectiles ($Z_1 = 2, 10$). For some other Z_1 and λ_0 similar results are also calculated and not shown here. One can see from the figure that although the classical and quamtum TCS are very close to each other for a large range of v, their discrepancy is quite clear for very low and high v regimes. Part of the relevant reason has been pointed out above. For very low velocity collisions, only the lowest several levels of partial wave ℓ's are involved since the de Broglie

wave length is long, the classical orbital picture is thus invalid for such a collison. At high v region the DCS for quantum and classical scattering of small angle is quite different, and the small angle scattering play a significant role to determine the TCS. This results in an obvious difference of TCS from classical and quantum mechanics.

V. CONCLUSION

In this paper, we examined the validity of classical mechanics to descibe the elastic ion-ion collision under repulsive Yukawa potential. Both results of classical and quantum DCSs are compared in detail as well as those of TCSs. The relevant results for the validity of classical mechanics are compared by the generalized Bohr's criterion (GBC). Our main conclusions are summarized as follows:

1. For very low-velocity collisions quantum and classical DCS are quite different in a large range of scattering angle. The reason is that the collision process is dominant by quantum wave effect in the case so that only very few partial waves contribute to the DCS. As velocity increases, the region that quantum and classical DCSs are different become smaller,which is towards to more and more small angle. This behavior agrees with the prediction of the not so strict GBC when $v < 2|Z_1 Z_2|$.

2. For low-velocity collisions quantum and classical TCSs are obviously different since the corresponding DCSs are quite different for a large range of scattering angle. As velocity increases, the discrepancy becomes negligible where the discrepancy between the corresponding DCSs in small angle has few affect to the TCS. However, when $v > 2|Z_1 Z_2|$, the discrepancy occurs again, since in such high velocity the small angle scattering

becomes dominant, which has an important affect upon the TCS.

3. The GBC is too strong to get a proper range where the clasical picture is reliable. Its weaker form Eq. (26) is invalid for very low velocity collision since the concept of impact parameter does not work in the case. Meanwhile in middle velocity range the weaker form can predict a reliable range where the clasical picture is reliable. The Bohr criterion does not work when $v > 2|Z_1Z_2|$, which coincides with its failure for Coulomb scattering for such velocity.

Anyhow, the difference between quantum and classical TCS has minor effects to the stopping power, the classical picture of ion-ion collision under ICF parameter is justified. Still, we hope that this paper serves as a reminder that the idea that ion-ion collision is a purely classical process should not be taken for granted but actually has deeper physical significance.

ACKNOWLEDGEMENT

REFERENCES

[1] D. S. Montgomery, W. S. Daughton, B. J. Albright, A. N. Simakov, D. C. Wilson, E. S. Dodd, R. C. Kirkpatrick, R. G. Watt, M. A. Gunderson, E. N. Loomis, E. C. Merritt, T. Cardenas, P. Amendt, J. L. Milovich, H. F. Robey, R. E. Tipton, and M. D. Rosen. Design considerations for indirectly driven double shell capsules. *Physics of Plasmas*, 25(9):092706, 09 2018.

[2] Chengliang Lin, Bin He, Yong Wu, and Jianguo Wang. A new efficient approach for the calculation of cross-sections with application to yukawa potential. *Plasma Physics and Controlled Fusion*, 65(5):055005, mar 2023.

[3] Zhen-Guo Fu, Zhigang Wang, Chongjie Mo, Dafang Li, Weijie Li, Yong Lu, Wei Kang, Xian-Tu He, and Ping Zhang. Stopping power of hot dense deuterium-tritium plasmas mixed with impurities to charged particles. *Phys. Rev. E*, 101:053209, May 2020.

[4] Zhigang Wang, Zhen-Guo Fu, Bin He, and Ping Zhang. Energy relaxation of multi-MeV protons traveling in compressed DT+Be plasmas. *Physics of Plasmas*, 21(7):072703, 07 2014.

[5] Lowell S. Brown, Dean L. Preston, and Robert L. Singleton Jr. Charged particle motion in a highly ionized plasma. *Physics Reports*, 410(4):237–333, May 2005.

[6] D. Wu, W. Yu, S. Fritzsche, and X. T. He. Particle-in-cell simulation method for macroscopic degenerate plasmas. *Phys. Rev. E*, 102:033312, Sep 2020.

[7] J. Zhang, W. M. Wang, X. H. Yang, D. Wu, Y. Y. Ma, J. L. Jiao, Z. Zhang, F. Y. Wu, X. H. Yuan, Y. T. Li, and J. Q. Zhu. Double-cone ignition scheme for inertial confinement fusion. *Philosophical Transactions of the Royal Society A: Mathematical, Physical and Engineering Sciences*, 378(2184):20200015, 2020.

[8] B. Z. Chen, D. Wu, J. R. Ren, D. H. H. Hoffmann, and Y. T. Zhao. Transport of intense particle beams in large-scale plasmas. *Phys. Rev. E*, 101:051203, May 2020.

[9] Peter Sigmund. Particle penetration and radiation effects, vol. 151 of springer series in solid-state sciences, 2006.

[10] Ejvind Bonderup. Penetration of charged particles through matter. *Lecture Notes, Institute of Physics and Astronomy, University of Aarhus*, 1981.

[11] Niels Bohr. *The penetration of atomic particles through matter*. Munksgaard Copenhagen, 1948.

[12] Jens Lindhard. Influence of crystal lattice on motion of energetic charged particles. *MKongel. Dan. Vidensk. Selsk., Mat.-Fys. Medd.*, 34(14), 1965.

[13] Ari Le, Adam Stanier, Lin Yin, Blake Wetherton, Brett Keenan, and Brian Albright. Hybrid-vpic: An open-source kinetic/fluid hybrid particle-in-cell code. *Physics of Plasmas*, 30(6), 2023.

[14] D. Wu, X. T. He, W. Yu, and S. Fritzsche. Monte carlo approach to calculate proton stopping in warm dense matter within particle-in-cell simulations. *Phys. Rev. E*, 95:023207, Feb 2017.

[15] C. O'Raifeartaigh and J.F. McGilp. Calculation of differential scattering cross-sections for classical binary elastic collisions. *Computer Physics Communications*, 28(3):255–264, 1983.

[16] Francesco Calogero. *Variable Phase Approach to Potential Scattering*. Elsevier, 1967.

[17] P. Mora. Coulomb logarithm accuracy in a yukawa potential. *Phys. Rev. E*, 102:033206, Sep 2020.

[18] Leonard S. Rodberg and R. M. Thaler. Introduction to the quantum theory of scattering. *American Journal of Physics*, 36(4):373–373, 1968.

[19] Ta-You Wu and Takashi Ohmura. *Quantum theory of scattering*. Courier Corporation, 2014.

[20] Lev Davidovich Landau and Evgenii Mikhailovich Lifshitz. *Quantum mechanics: non-relativistic theory*, volume 3. Elsevier, 2013.

[21] Peter Sigmund. Kinetic theory of particle stopping in a medium with internal motion. *Physical Review A*, 26(5):2497, 1982.

[22] E. M. Wright. Solution of the equation $ze^z = a$. *Bulletin of the American Mathematical Society*, 65(2):89–93, 1959.